Atmos. Chem. Phys. Discuss., 12, 15639–15674, 2012
www.atmos-chem-phys-discuss.net/12/15639/2012/
doi:10.5194/acpd-12-15639-2012

Atmospheric Chemistry and Physics Discussions

Impact of relative humidity and particles size distribution on aerosol light extinction in urban area of Guangzhou

Z. J. Lin[1,2], J. Tao[2,3], F. H. Chai[4], S. J. Fan[1], J. H. Yue[2], and L. H. Zhu[1,2]

[1]Department of Atmospheric Science, Sun Yat-Sen University, Guangzhou, China
[2]South China Institute of Environmental Sciences (SCIES), Guangzhou, China
[3]Department of Environmental Science, Sun Yat-Sen University, Guangzhou, China
[4]Chinese Research Academy of Environmental Sciences, Beijing, China

Received: 6 June 2012 – Accepted: 11 June 2012 – Published: 22 June 2012

Correspondence to: S. J. Fan (eesfsj@mail.sysu.edu.cn)

Published by Copernicus Publications on behalf of the European Geosciences Union.

Abstract

In urban area of Guangzhou, an experiment was conducted at the monitoring site of SCIES in order to recognize the impact of relative humidity (RH) and particles size distribution on aerosol light extinction during 2009 to 2010. Water-soluble ions and OC/EC in daily $PM_{2.5}$ samples was determined by the Dionex ion chromatography and the DIR model 2001 carbon analyzer, respectively; particles size distribution was measured by TSI 3321 APS; and total light scattering coefficient was measured by TSI 3565 Nephelometer. Inorganic salts that constitute $PM_{2.5}$ were recognized under an assumption of the electrical charge neutrality, while chemical components as POM, EC and water content were determined by means of hygroscopic growth calculation and chemical mass closure. As a result, $(NH_4)_2SO_4$, $NaNO_3$, POM, EC and water content were found to be the major components. By the Mie Model, light scattering and absorption coefficient of $PM_{0.5-2.5}$ were estimated on the basis of the chemical composition of $PM_{2.5}$ and the size distribution of number concentration of $PM_{0.5-2.5}$. This estimation was evaluated by results from Nephelometer measurement and proved to have high accuracy. With the knowledge of hygroscopic growth of some inorganic salts, it was realized that optical properties of $PM_{0.5-2.5}$ greatly depended on relative humidity, while light extinction was enhanced averagely 1.23, 1.38 and 1.75 times at 70 %, 80 % and 90 % RH, respectively. Moreover, light extinction coefficient of $PM_{0.5-2.5}$ increased averagely 1.24 to 1.28 times during wet days while merely 1.04 times in dry days. Furthermore, combined results from Nephelometer, the knowledge of relation between EC and aerosol light absorption and the Mie Model estimation, size distribution of total light extinction coefficient was determined. PM_1 contributed averagely 76 %, 85 %, 94 % and 93 % to light extinction in spring, summer, autumn and winter, respectively, while the contributions from $PM_{2.5}$ were 94 % at least.

ACPD
12, 15639–15674, 2012

1 Introduction

Atmospheric aerosol influences radiation budget of the earth-atmosphere system by scattering and absorbing solar radiation (Seinfeld and Spyros, 2006). Pollution caused by aerosol will enhance this light extinction effect. Furthermore, the aerosol impact on climate change will also be enhanced accordingly. With regard to the Mie Theory, to recognize size distribution of aerosol particle numbers and light extinction efficiency of a single particle are the keys to quantify light extinction effect (Seinfeld and Spyros, 2006). Aerosol absorbs water with an increasing relative humidity (RH). It should be taken into account in a place with a damp climate for this hygroscopic property will increase aerosol size and change optical properties of aerosol population. In the past century, scientists studied hygroscopic growth of some inorganic salts that constitute aerosol in order to quantify hygroscopic growth factor of aerosol population (Tang and Munkelwitz, 1994; Tang, 1996; Tang et al., 1997). Those studies related RH to aerosol size growth through laboratory measurement. Later on, a parallel observation with the Twin Differential Mobility Particle Sizer (TDMPS) and the Humidifying Differential Mobility Particle Sizer (H-DMPS) was used to directly measure particles size distribution and hygroscopic growth of the ambient aerosol particles smaller than 1 µm (Eichler et al., 2008). Moreover, with the combination of the Micro-Orifice Uniform Deposition Impactor (MOUDI); the Aerodynamic Particle Sizer (APS) and the knowledge of hygroscopic growth factor of some inorganic salts, it's able to determine particles size distribution and hygroscopic growth factor of the aerosol particles larger than 1 µm (Eichler et al., 2008).

Since socioeconomic developed in recent years, pollution caused by fine aerosol particles in Guangzhou and its surrounding area has attracted more and more attentions from the public and scientists. Lots of researches were carried out in order to illustrate the regional characteristic of aerosol chemical composition and the extent of visibility degradation due to aerosol light extinction (Wang et al., 2003; Bergin et al., 2004; Louie et al., 2005; Wu et al., 2005; Cao et al., 2007; Deng et al., 2008a, b; Tie

ACPD
12, 15639–15674, 2012

and Cao, 2009). Moreover, using methods mentioned above and the numerical simulation technique, integrated experiments of the PRIDE-PRD2004 in October 2004 and the PRIDE-PRD2006 in July 2006 were conducted in both urban and rural area of Guangzhou. These experiments focused on the formation mechanism of aerosol pollution including chemical transformation and driven force from regional meteorological condition (Fan et al., 2008; Su et al., 2008; Zhang et al., 2008a, b; Fan et al., 2011), size-resolve chemical composition and pollutant sources (Gnauk et al., 2008; Liu et al., 2008a, b; Jung et al., 2009; Xiao et al., 2010; Yu et al., 2010; Yue et al., 2010), mixing state of the EC and other non-light-absorption compound in aerosol (Cheng et al., 2006, 2008b), aerosol optical properties, radiative direct forcing and their RH dependence (Andreae et al., 2008; Cheng et al., 2008b; Eichler et al., 2008; Liu et al., 2010).

As well as in summer and autumn, it is necessary to characterize the temporal variation of aerosol light extinction effect in spring and winter regarding to the connection between meteorological condition and air pollution. To what extent, the weather during spring and winter in South China is frequently influenced by co-effects of cold air mass from the inland and warm air mass from the sea. Moreover, few studies were reported on a long term impact of RH and particles size distribution on aerosol light extinction in urban area of Guangzhou. For the purpose of an updated and complementary study on this topic, a series of experiment were carried out at the monitor site of SCIES during April 2009, July 2009, October 2009 and January 2010 representing spring, summer, autumn and winter, respectively, the results of these experiments are to be discussed in this paper.

ACPD
12, 15639–15674, 2012

2 Experimental

2.1 Monitoring site

The monitoring site of SCIES locates in Guangzhou city where geographical coordinates are 23°07′ N and 113°21′ E. It was designed for monitoring air quality influenced by pollutant regional transport and local sources emission. For this reason, instruments were installed on roof of the main building with a height of 53 m. This site was built with a clear vision over 300°, around which there is a residential area and a park about 500 m northeast to it. There does not seem to be any big source of air pollution but mobile emissions within circumference of 3 km. A satellite photo depicting the site's location and its surroundings is illustrated in Fig. 1. So far, data on aerosol samples, gaseous pollutants and meteorological parameters have been accumulated over a long period of time at this site. Previous works on the basis of these data can be read in open literatures (Tao et al., 2009, 2010, 2012).

2.2 Sampling and analysis

The measured aerosol properties and meteorological parameters during these experiments are listed in Table 1. The output from Nephelometer, APS and automatic weather station were hourly averaged before further analysis.

1. *$PM_{2.5}$ sampling.* During these experiments from 2009 to 2010, $PM_{2.5}$ samples were measured by an air sampler (BGI Corporation, Model PQ200) equipped with a cyclone that separates $PM_{2.5}$ particles from the aerosol population and with a vacuum pump that draws air at a rate of 16.7 l min^{-1}. The drawn airstream is connected to a 47 mm quartz filter (Whatman, QM-A). Before sampling, the quartz filters are baked at 800 °C for more than 3 h to remove adsorbed organic vapors, and then equilibrated in desiccators for 24 h. Prior to the measurement in ambient, the flow rate of $PM_{2.5}$ sampler is calibrated. Blank filters are collected and used to subtract the positive artifact caused by gas absorption. Finally, 123

ACPD
12, 15639–15674, 2012

daily quartz-filter samples with some blank ones were collected for every 23.5 h (starting at 10:00 LST each day and ending at 09:30 LST the following day). The analysis-ready samples were stored in a freezer at about −20 °C in case of particles volatilization.

2. *OC/EC determination.* A punch of 0.5 cm^2 from the collected quartz filter was analyzed for eight carbon fractions following the IMPROVE_A thermal/optical reflectance (TOR) protocol by a DIR model 2001 carbon analyzer (Atmoslytic Inc., Calabasas, CA) (Cao et al., 2007; Chow et al., 2007). This process produced four OC fractions (OC1, OC2, OC3 and OC4) at 140 °C, 280 °C, 480 °C and 580 °C, respectively, in a helium [He] atmosphere; OP (a pyrolyzed carbon fraction) was determined when transmitted laser light attained its original intensity after oxygen [O_2] added to that analysis atmosphere; and three EC fractions (EC1, EC2 and EC3) at 580 °C, 740 °C and 840 °C, respectively, in a (2 %) O_2/(98 %) [He] atmosphere. In practice, IMPROVE_TOR OC is defined as OC1 + OC2 + OC3 + OC4 + OP, while EC is defined as EC1 + EC2 + EC3 – OP (Chow et al., 2007). Inter-laboratory sample comparisons between applying the IMPROVE_TOR protocol and the TMO (thermal manganese dioxide oxidation) approach have shown the differences being lower than 5 % for TC and 10 % for OC and EC (Chow et al., 2007). Average field blanks were 1.8 and 0.1 μg m^{-3} for OC and EC, respectively.

3. *Water-soluble ions determination.* One quarter of the collected quartz filter sample was used to determine the mass concentrations of water-soluble ions. Four anions (SO_4^{2-}, NO_3^-, Cl^- and F^-) and five cations (Na^+, NH_4^+, K^+, Mg^{2+} and Ca^{2+}) in aqueous extracts from the filter were determined by ion chromatography (Dionex Corp, Sunnyvale, CA, Model Dionex 600). For these extractions, each sample was put into a separate 20 ml vial containing 10 ml distilled-deionised water (18 MΩ resistivity), and shaken first by an ultrasonic instrument for 60 min, then by mechanical shaker for 1 h for a complete extraction. The extracts were stored at 4 °C in a

ACPD
12, 15639–15674, 2012

pre-cleaned tube before further analysis. Cation (Na^+, NH_4^+, K^+, Mg^{2+} and Ca^{2+}) concentrations were determined with a CS12A column (Dionex Corp, Sunnyvale, CA.) and 20 mmol l^{-1} MSA eluent. Anions (SO_4^{2-}, NO_3^-, Cl^- and F^-) were separated by an AS11-HC column (Dionex Corp, Sunnyvale, CA) and 20 mmol l^{-1} KOH eluent. The limits of detection were less than 0.05 mg l^{-1} for both cations and anions. Standard reference materials produced by the National Research Centre for Certified Reference Materials in China were analyzed for quality assurance purposes. Blank values were subtracted from sample concentrations (Shen et al., 2009).

4. *Nephelometer deployment.* Total light scattering coefficient of aerosol was measured by an integrating Nephelometer (TSI Performance Measurement Tools, Model 3563) in wavelengths of 450 nm, 550 nm and 700 nm, respectively. Nephelometer calibration was performed by carbon dioxide (CO_2) as high-span gas and filtered air as low-span gas. Nephelometer draws ambient air through a temperature-controlled inlet at a flow rate of 20 l min^{-1}. The inner heater controls the RH of aerosol intake at a level lower than nearly 70 %. The output data were set to 1 min averaged in these experiments, and zero level data was measured continuously for 5 min after each hourly (60 min) sampling.

5. *APS deployment.* Size distribution of number concentration of aerosol was measured by APS (TSI Aerodynamic Sizer, Model 3321) with 52 size bins in diameter range from 0.5–20 µm by determining time-of-flight of individual particle in an accelerating flow field. A drying tube was added before drawing air to capture dry aerosol. Flow rate of 5 l min^{-1} and 5 min data averaged were set in APS operation.

6. *Weather station deployment.* Ambient relative humidity had been recorded by an automatic weather station (VASALA Model QMH102) installed 3 m above the roof.

ACPD
12, 15639–15674, 2012

3 Methodology

3.1 Chemical component determination

Recognizing chemical compounds that constitute aerosol particles is necessary for determining the thermodynamic and optical properties of aerosol population. For fine aerosol, components include inorganic salts, POM, EC and the water taken up by the salts.

3.1.1 Inorganic salt

Under an assumption of the electrical charge neutrality (Eichler et al., 2008), identification to associations among the water-soluble ions raised a recognition of the inorganic salts. The cations identified from $PM_{2.5}$ samples were Na^+, NH_4^+, K^+, Mg^{2+} and Ca^{2+}, while the anions were SO_4^{2-}, NO_3^- and Cl^-.

In the light of previous studies (Seinfeld and Spyros, 2006; Cheng et al., 2008c; Han et al., 2009; Yue et al., 2011), it is usually considered that for fine particles: (1) NH_4^+, SO_4^{2-} and NO_3^- are mainly from secondary transformations, and NH_4^+ associates with SO_4^{2-} to become $(NH_4)_2SO_4$, if any remains, then it associates with NO_3^- to become NH_4NO_3; (2) biomass burn is responsible for K^+ and Cl^-, K^+ associates with Cl^- to become KCl, if any remains, then it associates with SO_4^{2-} to become K_2SO_4; (3) Na^+ associates with Cl^- in sea salt to become NaCl. However, NaCl will react with gaseous nitric acid to produce sodium nitrate in the process of atmospheric diffusion. Hence Na^+ associates with NO_3^- to become $NaNO_3$, if any remains, then it associates with SO_4^{2-} to become Na_2SO_4; (4) sea salt and soil are the sources of Mg^{2+} and Ca^{2+}. Ca^{2+} associates with NO_3^-, if any remains, it associates with SO_4^{2-} and Cl^- in succession. It's the similar case with Mg^{2+}. Following these associations, inorganic salts including $(NH_4)_2SO_4$, NH_4NO_3, $NaNO_3$, Na_2SO_4, KCl, NaCl, $Ca(NO_3)_2$, $Mg(NO_3)_2$, K_2SO_4 and $CaSO_4$ can be recognized.

ACPD
12, 15639–15674, 2012

3.1.2 POM and water content

As recommended in a previous study (Hand and Malm, 2006), a factor of 1.8 for urban area was adapted to "convert" the mass of OC to that of POM. Since POM, EC and other unidentified components were considered to have no hygroscopic growth, the mass of water taken up by inorganic salts can be estimated based on hygroscopic growth factors of inorganic salts following Eq. (1) where m_w and ρ_w is mass concentration and density of water uptake, respectively. Moreover, V_j stands for the volume of the j-th inorganic salts in aerosol, while $f_{g,j}$ is the hygroscopic growth factor at a specified RH.

$$m_w = \rho_w \cdot \sum_j V_j \cdot \left(f_{g,j}^3 - 1\right) \quad (1)$$

For the $PM_{2.5}$ samples were weighted in laboratory condition of 40 % RH, the inorganic salts, POM, EC and water content were determined at this RH as well. Hence, the unidentified part in $PM_{2.5}$, named the Residual, can be determined from the difference between the total mass and the sum mass of the identified part. Similarly, the mass of aerosol at arbitrary RH can be determined into two parts. One is the salts, POM, EC and the Residual at 40 % RH, while the other one is the water uptake at that desired RH.

3.2 Light scattering and absorption coefficient estimation

In consideration of instrumental deployment during these experiments, it is likely to introduce the internal mixing, one of simplifications about aerosol mixing status (Seinfeld and Spyros, 2006; Cheng et al., 2008c), into the Mie Model to estimate the extent of aerosol light scattering and absorption coefficient. The aerosol optical properties to discuss later are referenced to the light of 550 nm wavelength, only exceptions will be noted.

ACPD
12, 15639–15674, 2012

3.2.1 EORI and EGF

The EORI (Effective Optical Refractive Index) represents the averaged ORI of internally mixing aerosol population, which can be calculated with the ORIs of each chemical component in aerosol following mixing rules of Volume Average (Lesins et al., 2002). This mixing rule considers relationship among each chemical component as equally weighed by their volumes, the formulas of which were written as Eq. (2) and Eq. (3).

$$n_{\text{eff}} = \left(\sum_j n_j \cdot m_j/\rho_j\right) \Big/ \left(\sum_j m_j/\rho_j\right) \tag{2}$$

$$k_{\text{eff}} = \left(\sum_j k_j \cdot m_j/\rho_j\right) \Big/ \left(\sum_j m_j/\rho_j\right) \tag{3}$$

In Eqs. (2) and (3), m_j stands for the mass of the j-th component in aerosol, while ρ_j is the density. Respectively, n_j is the real part of ORI of the j-th component, k_j is the imaginary part. For the EORI, n_{eff} is the real part, and k_{eff} is the imaginary part.

The EGF (Effective Hygroscopic Growth Factor) was the averaged hygroscopic growth factor of internally mixing aerosol, which can be calculated with f_g of each chemical component in aerosol following Zdanovskii-Stokes-Robinson assumption (Stokes and Robinson, 1966). It can be depicted by Eq. (4).

$$f_{\text{eff}} = \left(\sum_j a_j \cdot f_{g,j}^3\right)^{1/3} \tag{4}$$

In Eq. (4), f_{eff} is the EGF. a_j is the volume fraction of the j-th component in aerosol, while $f_{g,j}$ is the hygroscopic growth factor. The f_g of some inorganic salts had been determined in previous studies (Tang and Munkelwitz, 1994; Tang, 1996; Kelly and Wexler, 2006) where related f_g to ambient RH by laboratory measurements.

ACPD
12, 15639–15674, 2012

3.2.2 Mie Model estimation

According to the Mie Theory, b_{sp} (light scattering coefficient) and b_{ap} (light absorption coefficient) can be estimated with Eqs. (5) and (6), respectively (Bohren et al., 1998; Seinfeld and Spyros, 2006).

$$b_{sp} = \sum_j b_{sp,j} = \sum_j \frac{\pi D_j^2}{4} \cdot Q_{sp,j} \cdot N_j \quad (5)$$

$$b_{ap} = \sum_j b_{ap,j} = \sum_j \frac{\pi D_j^2}{4} \cdot Q_{ap,j} \cdot N_j \quad (6)$$

$$D_j = \frac{D_{a,j}}{\sqrt{\rho_{dry}}} \cdot f_{eff} \quad (7)$$

In Eqs. (5) and (6), D_j stands for the midpoint Stokes diameter in the j-th size range of aerosol, while N_j is the number concentration of aerosol population with diameter D_j. Equation (7) converted $D_{a,j}$ from APS size bin to D_j required by the Mie Model, and the N_j corresponding to $D_{a,j}$ were from APS measurement. Moreover, the f_{eff} in Eq. (7) was used to estimate the hygroscopic growth of D_j under an assumption that no change in particles number concentration in the process of hygroscopic growth. $Q_{sp,j}$ represents light scattering efficiency of a single particle with diameter D_j, while $Q_{ap,j}$ represents light absorption efficiency. At a given light wavelength, they both are the functions of D_j and the EORI. Density of dry aerosol population, ρ_{dry}, in Eq. (7) can be calculated with Eq. (8) where ρ_j is density of the j-th chemical components without water uptake. Wet aerosol density, ρ_{wet} in Eq. (9), can also be calculated with Eq. (8)

ACPD
12, 15639–15674, 2012

where water was included. Additionally, wet aerosol mass concentration, m_{wet}, can be calculated with Eq. (9).

$$\rho = \left(\sum_j m_j\right) \Big/ \left(\sum_j m_j/\rho_j\right) \tag{8}$$

$$m_{wet} = \rho_{wet} \cdot \sum_j \frac{\pi D_j^3}{6} \cdot N_j \tag{9}$$

Practically, it's able to estimate $b_{sp,pm0.5–2.5}$ by the Mie Model based on the EORI, EGF of $PM_{2.5}$ and $N_{j,pm0.5–2.5}$ from APS measurement. In order to evaluate the accuracy of this estimation, a correlation analysis was performed between temporal variations of $b_{sp,pm0.5–2.5}$ from the estimation and $b_{sp,neph}$ (550 nm) from Nephelometer measurement. By considering an evaluation with higher temporal resolution, these two data sets should be compared with each other in hourly average. However, under the circumstance of no available data about diurnal variation of chemical composition, the required hourly EORI, EGF and ρ_{dry} were valued to their daily averages which were determined from chemical composition of daily $PM_{2.5}$ sample. Furthermore, hourly values of $b_{sp,neph}$ (550 nm) were corrected with an approach stated in a previous study (Anderson and Ogren, 1998) where used a linear function of Angstrom exponent $å_{450/700}$ ($å_{450/700}$ was calculated with $b_{sp,neph,450\,nm}$ and $b_{sp,neph,700\,nm}$) as correction factors for Angular Nonidealities. It is noted that the EGF adapted in this evaluation was calculated at the RH detected by Nephelometer built-in RH sensor rather than in ambient condition.

3.2.3 RH dependence

For convenience, it is defined that $h_Y(RH) = Y(RH)/Y(RH_0)$ where Y(RH) stands for a specified property of aerosol at arbitrary RH. RH_0 is a referenced RH at which aerosol

ACPD
12, 15639–15674, 2012

is considered to be relative dry or without obvious hygroscopic growth. Hence, h_Y is a factor that quantifies the extent of hygroscopic growth. In the light of a previous study (Cheng et al., 2008b), the RH dependence of h_Y can be fitted by a few functions including Eqs. (10), (11) and (12). Having something in common, these three functions are monotone and ensure h_Y to be unity at RH_0. However, comparing the power part among them, Eq. (11) and (12) can better fit an RH dependence pattern where hygroscopic growth activates at high RH level.

$$h_Y(RH) = \left(\frac{1 - RH}{1 - RH_0}\right)^a \quad (10)$$

$$h_Y(RH) = \left(\frac{1 - RH}{1 - RH_0}\right)^{a\cdot(RH - RH_0)} \quad (11)$$

$$h_Y(RH) = \left(\frac{1 - RH}{1 - RH_0}\right)^{a\cdot RH} \quad (12)$$

3.2.4 Size distribution

For the purpose of determining the light extinction contribution from aerosol in different size, it's necessary to estimate the mass concentration of $PM_{0.5}$, $PM_{0.5-1}$, $PM_{1-2.5}$ and $PM_{2.5-20}$, then, the b_{sp} and b_{ap} of them. Regarding daily average, the $b_{sp,pm0.5-2.5}$, $b_{ap,pm0.5-2.5}$ and $m_{pm0.5-2.5}$ can be estimated by the Mie Model based on the chemical composition of $PM_{2.5}$ and size distribution of $N_{pm0.5-2.5}$ at ambient RH. Regardless of the difference in chemical composition, it's feasible to estimate $b_{sp,pm2.5-20}$, $b_{ap,pm2.5-20}$ and $m_{pm2.5-20}$ by the Mie Model on the basis of size distribution of $N_{pm2.5-20}$. Furthermore, $b_{sp,pm0.5}$, $b_{ap,pm0.5}$ and $m_{pm0.5}$ can be estimated by Eqs. (13), (14) and (15). $m_{pm2.5}$ in Eq. (13) was the mass concentration of daily $PM_{2.5}$ sample in ambient RH

ACPD
12, 15639–15674, 2012

condition, while $b_{sp,neph}$ in Eq. (14) was corrected to its value at ambient RH. Referenced to a previous study (Wu et al., 2009), $b_{ap,pm2.5} = 8.28\, m_{ec} + 2.23$ in Eq. (15).

$$m_{pm0.5} = m_{pm2.5} - m_{pm0.5-2.5} \tag{13}$$

$$b_{sp,pm0.5} = b_{sp,neph} \cdot \left(\frac{b_{sp,pm0.5-2.5}, RH_{Ambient}}{b_{sp,pm0.5-2.5}, RH_{Nephelometer}} \right) - b_{sp,pm0.5-2.5} - b_{sp,pm2.5-20} \tag{14}$$

$$b_{ap,pm0.5} = b_{ap,pm2.5} - b_{ap,pm0.5-2.5} \tag{15}$$

4 Results and discussion

4.1 Mie Model estimation and its evaluation

Temporal variations of mole proportion of the identified water-soluble ions in $PM_{2.5}$ are illustrated in Fig. 2. On the whole, the cations were sufficient to neutralize the anions in every sample, while SO_4^{2-} and NH_4^+ had large amount but Mg^{2+} was hardly any. In spring, there's hardly any Ca^{2+} while NH_4^+ and NO_3^- were high in proportion. During summer, Na^+, Ca^{2+} and Cl^- raised their proportions while NH_4^+ and K^+ lowered theirs. SO_4^{2-} reached its maximum in autumn while NO_3^- and Cl^- stayed in low level. NH_4^+, K^+, Cl^- and NO_3^- were high in proportion during winter.

Inorganic salts, POM, EC and the water content were determined based on methods discussed earlier, the temporal variations of which in mass proportion are illustrated in Fig. 3. Despite of temporal variation, $(NH_4)_2SO_4$, $NaNO_3$, POM and EC were the major components for their considerable amount in proportion along the experiment.

ACPD
12, 15639–15674, 2012

Regarding other salts, Na_2SO_4 and NaCl raised their amount in both summer and early autumn. For the compounds of Ca^{2+}, it was in the form of $CaSO_4$ in summer and autumn, while $Ca(NO_3)_2$ in winter. It is for certain that the amount of water content was relative low in dry days in autumn. To what extent, there was a linear relation between POM and EC, and their proportions were higher in summer and autumn than in spring and winter. Limited to laboratory equipments, there were still 13 to 23 % in total mass, the Residual, where chemical composition can't be determined

The optical parameters of chemical components for calculating the EORI were learned from some open literatures (Tang, 1996; Chazette and Louisse, 2001; Sloane, 1986; Haynes, 2011; Seinfeld and Spyros, 2006; Eichler et al., 2008) and are listed in Table 2. As illustrated in Fig. 4, those inorganic salts with determined f_g including NH_4NO_3, NaCl, $(NH_4)_2SO_4$, Na_2SO_4, $NaNO_3$, KCl were plotted in the form of their RH dependence curves. For those inorganic salts without determined f_g, it's reasonable to neglect their hygroscopic growth as their volume concentration were small enough in this case. Moreover, the EGF of $PM_{2.5}$ samples were calculated and their average over a span of four months is plotted in the form of RH dependence curve in Fig. 4. Discontinuities in this curve were due to the f_g considered to be unity when ambient RH dropped to a specified salt's crystallization point. Example is the one at 37 % RH which is the crystallization point of $(NH_4)_2SO_4$. On the basis of the methods discussed earlier, the EORI, EGF and density of dry/wet aerosol were calculated and the statistics of the results are listed in Table 3.

Regarding the Mie model evaluation mentioned above, as illustrated in Fig. 5, correlation coefficients between the $b_{sp,pm0.5\text{-}2.5}$ from the estimation and $b_{sp,neph}$ from Nephelometer were found to be 0.81, 0.87, 0.73 and 0.80 at 0.05 significant levels in spring, summer, autumn and winter, respectively. With this implication of a coherent temporal variation between model estimation and direct measurements, it's reliable to estimate $b_{sp,pm0.5–2.5}$ with high accuracy by applying the Mie Model based on APS measurement and $PM_{2.5}$ sampling.

ACPD
12, 15639–15674, 2012

4.2 RH dependence of optical property of $PM_{0.5–2.5}$

Figure 4 illustrates that f_{eff} increased more rapidly after ambient RH over 37 %, it's reasonable to set $RH_0 = 37\,\%$ in Eq. (10) to Eq. (12). By the Mie Model estimation, RH dependence patterns of $h_{bep,pm0.5–2.5}$ (light extinction coefficient is denoted as b_{ep}, it is the sum of b_{sp} and b_{ap}), $h_{bsp,pm0.5–2.5}$, $h_{bap,pm0.5–2.5}$ and $h_{\omega 0,pm0.5–2.5}$ (single scattering albedo is denoted as ω_0, it is the ratio of b_{sp} to b_{ep}) were determined and plotted in Fig. 6. It was found that Eq. (10) best fitted RH dependence patterns of $h_{bep,pm0.5–2.5}$, $h_{bsp,pm0.5–2.5}$ and $h_{\omega 0,pm0.5–2.5}$. Parameter "a" and the R^2 of these curve fittings by Eq. (10) are listed in Table 4. On the contrary, $h_{bap,pm0.5–2.5}$ fluctuated around 1.00 when RH increased from 37 % to 66 %, and then began to drop. It made none of Eqs. (10), (11) and (12) able to fit that RH dependence pattern. Moreover, Table 4 shows hygroscopic growth enhanced $b_{ep,pm0.5–2.5}$ averagely 1.23, 1.38 and 1.75 times at 70 %, 80 % and 90 % RH, respectively. Regarding temporal variation of ambient RH, autumn was a relative dry season in South China while the other three were categorized to wet seasons. Table 5 shows that $b_{ep,pm0.5–2.5}$ was enhanced by hygroscopic growth averagely 1.24 to 1.28 times during wet seasons and merely 1.04 times in dry season.

4.3 Size distribution of mass concentration and light extinction coefficient

Regarding the monthly average noted in Table 6, the maximum of both m_{total} and $b_{ep,total}$ was in winter while the minimum of them was in summer. Implied from a low ω_0, light absorption effect in summer was strengthened. A low $\mathring{a}_{450/700}$ indicated the size of particles that constitute the aerosol population was larger in spring than in the other seasons. In order to recognize mass efficiency of light scattering and absorption, $e_{sp} = b_{sp}\,m^{-1}$ and $e_{ap} = b_{ap}\,m^{-1}$ are defined. A low $e_{sp,total}$ and a high $e_{ap,total}$ supported the enhanced light absorption in summer. Moreover, the sum of e_{sp} and e_{ap} indicated mass efficiency of light extinction was higher in autumn and winter.

ACPD
12, 15639–15674, 2012

Temporal variations of size distribution of m_{total} and $b_{ep,total}$ are illustrated in Fig. 7. PM_1 contributed 58 to 79 % in total mass and 76 to 94 % in light extinction, while $PM_{2.5}$ did 78 to 88 % contributions to the total mass and 94 to 98 % to light extinction. Sharing a similarity with the low $\mathring{a}_{450/700}$ in spring, $PM_{0.5–2.5}$ gained much weight and carried much contributions to $b_{sp,total}$ through hygroscopic growth. Implied from size distribution of e_{sp} and e_{ap} illustrated in Fig. 8, large particles were more efficient in light absorption but less in light scattering than small ones.

With a less consideration of anthropogenic emissions varying much during these experiments, a low m_{total} and $b_{ep,total}$ in summer was probably due to a meteorological condition in favor of a diffusion or removal of air pollutants. As the proportion of m_{ec} varied relative little, an aged air mass from the sea containing more internal mixing EC explained a higher light absorption during summer. This conclusion was supported by a previous study (Cheng et al., 2006). Moreover, the high mass proportion of Na^+ in summer was an evidence for that air mass from the sea. On the other hand, m_{total} and $b_{ep,total}$ increased much in spring, autumn and winter. Aerosol population gained more weight and its light extinction was enhanced through humidification in spring. Owing to $PM_{0.5}$ having much weight and its high mass scattering efficiency, $b_{ep,total}$ was even higher while m_{total} was a bit lower in autumn than in spring. It indicated that hygroscopic growth had notable contributions to the rising of light extinction effect in spring, while ultra-fine particles accumulation accounted for that rising during dry days in autumn. Co-effects of hygroscopic growth and particles accumulation took account for the high $b_{ep,total}$ and m_{total} in winter.

5 Summary and conclusion

With regard to aerosol population in internal mixing status, $b_{ep,pm0.5–2.5}$ can be estimated with high accuracy by the Mie Model. The EORI and EGF required in this estimation can be calculated on the ground of chemical composition of $PM_{2.5}$. With a damp climate in Guangzhou, $b_{ep,pm0.5–2.5}$ greatly depended on ambient RH and was

ACPD
12, 15639–15674, 2012

enhanced up to nearly 2 times from 37 % to 92 % RH. Averagely, hygroscopic growth factor of $b_{ep,pm0.5–2.5}$ was 1.24 to 1.28 during wet days and merely 1.04 in dry days. Combined Nephelometer measurement, mass concentration of EC and the Mie Model estimation, contributions to b_{ep} from aerosol in different size can be estimated. PM_1 contributed averagely 76 %, 85 %, 94 % and 93 % to b_{ep} in spring, summer, autumn and winter, respectively, while the contributions from $PM_{2.5}$ were 94 % at least. Strong atmospheric diffusion may be in favor of a low b_{ep} in summer. Hygroscopic growth carried notable contribution to the rising of b_{ep} during wet days in spring, while ultrafine particles accumulation was responsible for that rising during dry days in autumn. The b_{ep} stay high in winter as the consequence to the co-effects of the high RH level and fine aerosol pollution. Implied from the discussion in this paper, regional meteorological condition such as surface wind field pattern may govern the pollutant regional transport which resulted in the temporal variations of aerosol chemical composition. An investigation on this will be carried out in a near study.

Acknowledgements. This work was supported by Commonwealth and Environmental Protection Project of the Ministry of Environmental Protection of the People's Republic of China (200809143); China National Basic Research and Development Program (2002CB410801 and 2011CB403403) and National Natural Science Foundation (40875007).

References

Anderson, T. L. and Ogren, J. A.: Determining Aerosol Radiative Properties Using the TSI 3563 Integrating Nephelometer, Aerosol Sci. Tech., 29, 57–69, 1998.

Andreae, M. O., Schmid, O., Yang, H., Chand, D., Yu, J. Z., Zeng, L. M., and Zhang, Y. H.: Optical properties and chemical composition of the atmospheric aerosol in urban Guangzhou, China, Atmos. Environ., 42, 6335–6350, 2008.

Bergin, M., Hagler, G., Salmon, L., Zheng, M., Chameides, W., Kiang, C. S., Schauer, J., and Yu, J.: Fine particulate Matter ($PM_{2.5}$) in the Pearl River Delta. Project 2 Scientific Report to the Hong Kong Civic Exchange, 2004.

ACPD

12, 15639–15674, 2012

Bohren, C. F. and Huffman, D. R.: Absorption and scattering of light by small particles, John Wiley & Sons, Inc., 1998.

Cao, J. J., Lee, S. C.,Chow, J. C.,Watson, J. G., Ho, K. F., Zhang, R. J., Jin, Z. D., Shen, Z.X., Chen, G. C., Kang, Y.M., Zou S.C., Zhang L.Z., Qi, S. H., Dai, M.H., Cheng, Y., and Hu, K.: Spatial and seasonal distributions of carbonaceous aerosols over China, J. Geophys. Res., 112, D22S11, doi:10.1029/2006JD008205, 2007.

Chazette, P. and Liousse, C.: A case study of optical and chemical ground apportionment for urban aerosols in Thessaloniki, Atmos. Environ., 35, 2497–2506, 2001.

Cheng, Y. F., Eichler, H., Wiedensohler, A., Heintzenberg, J., Zhang, Y. H., Hu, M., Herrmann, H., Zeng, L. M., Liu, S., Gnauk, T., Bruggemann, E., and He, L. Y.: Mixing state of elemental carbon and non-light-absorbing aerosol components derived from in situ particle optical properties at Xinken in Pearl River Delta of China, J. Geophys. Res., 111, D20204, doi:10.1029/2005JD006929, 2006.

Cheng, Y. F., Wiedensohler, A., Eichler, H., Su, H., Gnauk, T., Brüggemann, E., Herrmann, H., Heintzenberg, J., Slanina, J., Tuch, T., Hu, M., and Zhang, Y. H.: Aerosol optical properties and related chemical apportionment at Xinken in Pearl River Delta of China, Atmos. Environ., 42, 6351–6372, 2008a.

Cheng, Y. F., Wiedensohler, A., Eichler, H., Heintzenberg, J., Tesche, M., Ansmann, A., Wendisch, M., Su, H., Althausen, D., Herrmann, H., Gnauk, T., Bruggemann, E., Hu, M., and Zhang, Y. H.: Relative humidity dependence of aerosol optical properties and direct radiative forcing in the surface boundary layer at Xinken in Pearl River Delta of China: An observation based numerical study, Atmos. Environ., 42, 6373–6397, 2008b.

Cheng, Y. F., Zhang, Y. H., Hu, M., and Wiedensohler, A.: An observation-based method for investigating the atmospheric aerosol radiative properties in pearl river delta of China, http://www.sciencep.com, China, 2008c.

Chow, J. C., Watson, J. G., Chen, L. W., Chang, M. C., Robinson, N. F., Trimble, D., and Kohl, S.: The IMPROVE_A temperature protocol for thermal/optical carbon analysis: maintaining consistency with a long-term database, J. Air Waste Manage., 57, 1014–1023, 2007.

Deng, X. J., Tie, X. X., Zhou, X. J., Wu, D., Zhong, L. J., Tan, H. B., Li, F., Huang, X. Y., Bi, X. Y., and Deng, T.: Effects of Southeast Asia biomass burning on aerosols and ozone concentrations over the Pearl River Delta (PRD) region, Atmos. Environ., 42, 8493–8501, 2008a.

ACPD

12, 15639–15674, 2012

Deng, X. J., Tie, X. X., Wu, D., Zhou, X. J., Bi, X. Y., Tan, H. B., Li, F., and Jiang, C. L.: Long-term trend of visibility and its characterizations in the Pearl River Delta (PRD) region, China, Atmos. Environ., 42, 1424–1435, 2008b.

Eichler, H., Cheng, Y. F., Birmili, W., Nowak, A., Wiedensohler, A., Brüggemann, E., Guauk, T., Herrmann, H., Althausen, D., Ansmann, A., Engelmann, R., Tesche, M., Wendisch, M., Zhang, Y. H., Hu, M., Liu, S., and Zeng, L. M.: Hygroscopic properties and extinction of aerosol particles at ambient relative humidity in South-Eastern China, Atmos. Environ., 42, 6321–6334, 2008.

Fan, S. J., Wang, B. M., Teshce, M., Engelmann, R., Althausen, A., Liu, J., Zhu, W., Fan, Q., Li, M. H., Ta, N., Song, L. L., and Leong, K. L.: Meteorological conditions and structures of atmospheric boundary layer in October 2004 over Pearl River Delta area, Atmos. Environ., 42, 6174–6186, 2008.

Fan, S. J., Fan, Q., Yu, W., Luo, X. Y., Wang, B. M., Song, L. L., and Leong, K. L.: Atmospheric boundary layer characteristics over the Pearl River Delta, China, during the summer of 2006: measurement and model results, Atmos. Chem. Phys., 11, 6297–6310, doi:10.5194/acp-11-6297-2011, 2011.

Guauk, T., Muller, K., Pinxteren, D., He, L. Y., Niu, Y., Hu, M., and Herrmann, H.: Size-segregated particulate chemical composition in XinKen, Pearl River Delta, China: OC/EC and organic compounds, Atmos. Environ., 42, 6296–6309, 2008.

Han, Y. M., Shen, Z. X., Cao, J. J., Li, X. X., Zhao, J. L., Liu, P. P., Wang, Y. H., and Zhou, J.: Seasonal variations of water-soluble inorganic ions in atmospheric particles over Xi'an, Environ. Chem., 28, 261–266, 2009.

Hand, J. L. and Malm, W. C.: Review of the IMPROVE equation for estimating ambient light extinction coefficients. Cooperative Institute for Research in the Atmosphere, Colorado State University, ISSN 0737-5352-71, 2006.

Haynes, W. M. (Ed.): CRC Handbook of Chemistry and Physics 92nd Edition, CRC Press, 2011.

Kelly, J. T. and Wexler, A. S.: Water uptake by aerosol: Water activity in supersaturated potassium solutions and deliquescence as a function of temperature, Atmos. Environ., 40, 4450–4468, 2006.

Lesins, G., Chylek, P., and Lohman, U.: A study of internal and external mixing scenarios and its effect on aerosol optical properties and direct radiative forcing, J. Geophys. Res., 107, 4094, doi:10.1029/2001JD000973, 2002.

ACPD

12, 15639–15674, 2012

Liu, S., Hu, M., Slanina, S., He, L. Y., Niu, Y. W., Bruegemann, E., Gnauk, T., and Herrmann, H.: Size distribution and source analysis of ionic compositions of aerosols in polluted periods at Xinken in Pearl River Delta (PRD) of China, Atmos. Environ., 42, 6284–6295, 2008a.

Liu, X. G., Cheng, Y. F., Zhang, Y. H., Jung, J., Sugimoto, N., Chang, S. Y., Kim, Y. J., Fan, S. J., and Zeng, L. M.: Influences of relative humidity and particle chemical composition on aerosol scattering properties during the 2006 PRD campaign, Atmos. Environ., 42, 1525–1536, 2008b.

Liu, X. G., Zhang, Y. H., Wen, M. T., Wang, J. L., Jung, J. S., Chang, S. Y., Hu, M., Zeng, L. M., and Kim, Y. J.: A Closure Study of Aerosol Hygroscopic Growth Factor during the PRD 2006 Campaign, Adv. Atmos. Sci., 27, 947–956, doi:10.1007/s00376-009-9150-z, 2010.

Jung, J. S., Lee, H., Kim, Y. J., Liu, X. G., Zhang, Y. H., Gu, J. W., and Fan, S. J.: Aerosol chemistry and the effect of aerosol water content on visibility impairment and radiative forcing in Guangzhou during the 2006 Pearl River Delta campaign, J. Environ. Manage., 90, 3231–3244, 2009.

Louie, P. K. K., Waston, J. G., and Chow, J. C.: Seasonal characteristics and regional transport of $PM_{2.5}$ in Hong Kong, Atmos. Environ., 39, 1695–1710, 2005.

Seinfeld, J. H. and Spyros, N. P.: Atmospheric Chemistry and Physics: from air pollution to climate change (Second Edition), John Wiley & Sons Inc., New York, 2006.

Shen, Z. X., Arimoto, R., Cao, J. J., Zhang, R. J., Li, X. X., Du, N., Tomoaki, O., Shunsuke, N., and Shigeru, T.: Seasonal variations and evidence for the effectiveness of pollution controls on water-soluble inorganic species in total suspended particulates and fine particulate matter from Xi'an, China, J. Air Waste Manage., 58, 1560–1570, 2008.

Sloane, C. S.: Effect of composition on aerosol light scattering efficiencies, Atmos. Environ., 20, 1025–1037, 1986.

Stokes, R. H. and Robinson, R. A.: Interactions in aqueous nonelectrolyte solutions. I. Solute-solvent equilibria, J. Phys. Chem., 70, 2126–2131, 1966.

Su, H., Cheng, Y. F., Cheng, P., Zhang, Y. H., Dong, S. F., Zeng , L. M., Wang, X. S., Slanina, J., Shao, M., and Wiedensohler, A.: Observation of nighttime nitrous acid (HONO) formation at a non-urban site during PRIDE-PRD2004 in China, Atmos. Environ., 42, 6219–6232, 2008.

Tang, I. N.: Chemical and size effects of hygroscopic aerosols on light scattering coefficients, J. Geophys. Res., 101, 19245–19250, 1996.

ACPD
12, 15639–15674, 2012

Tang, I. N. and Munkelwitz, H. R.: Water activities, densities, and refractive indices of aqueous sulfates and sodium nitrate droplets of atmospheric importance, J. Geophys. Res., 99, 18801–18808, 1994.

Tang, I. N., Tridico, A. C., and Fung, K. H.: Thermodynamic and optical properties of sea salt aerosols, J. Geophys. Res., 102, 23269–23275, 1997.

Tao, J., Ho, K. F., Chen, L. G., Zhu, L. H., Han, J. L., and Xu, Z. C.: Effect of chemical composition of $PM_{2.5}$ on visibility in Guangzhou, China, 2007 spring, Particuology, 7, 68–75, 2009.

Tao, J., Zhang, R. J., Dong, L., Zhang, T., Zhu, L. H., Han, J. L., Xu, Z. C.: Characterization of Water-soluble Inorganic ions in $PM_{2.5}$ and PM_{10} in Summer in Guangzhou, Environ. Sci., 31, 1417–1424, 2010.

Tao, J., Cao, J. J., Zhang, R. J., Zhu L. H., Zhang, T., Shi, S., and Chan, C. Y.: Reconstructed light extinction coefficients using chemical compositions of $PM_{2.5}$ in winter in Urban Guangzhou, China, Adv. Atmos. Sci., 29, 359–368, 2012.

Tie, X. X. and Cao, J. J.: Aerosol pollution in China: Present and future impact on environment, Particuology, 7, 426–431, 2009.

Wang, T., Poon, C. N., Kwok, Y. H., and Li, Y. S.: Characterizing the temporal variability and emission patterns of pollution plumes in the Pearl River Delta of China, Atmos. Environ., 37, 3539–3550, 2003.

Wu, D., Tie, X. X., Li, C. C., Ying, Z. M., Lau, A., Huang, J., Deng, X. J., and Bi, X. Y.: An extremely low visibility event over the Guangzhou region: a case study, Atmos. Environ., 39, 6568–6577, 2005.

Wu, D., Mao, J. T., Deng, X. J., Tie, X. X., Zhang, Y. H., Zeng, L. M., Li, F., Tan, H. B., Bi, X. Y., Huang, X. Y., Cheng, J., and Deng, T.: Black carbon aerosols and their radiative properties in the Pearl River Delta region, Sci. China Ser. D, 52, 1152–1163, 2009.

Xiao, R., Takegawa, N., Zheng, M., Kondo, Y., Miyazaki, Y., Miyakawa, T., Hu, M., Shao, M., Zeng, L., Gong, Y., Lu, K., Deng, Z., Zhao, Y., and Zhang, Y. H.: Characterization and source apportionment of submicron aerosol with aerosol mass spectrometer during the PRIDE-PRD 2006 campaign, Atmos. Chem. Phys., 11, 6911–6929, doi:10.5194/acp-11-6911-2011, 2011.

Yu, H., Wu, C., Wu, D., and Yu, J. Z.: Size distributions of elemental carbon and its contribution to light extinction in urban and rural locations in the pearl river delta region, China, Atmos. Chem. Phys., 10, 5107–5119, doi:10.5194/acp-10-5107-2010, 2010.

ACPD

12, 15639–15674, 2012

Yue, D. L., Hu, M., Wu, Z. J., Guo, S., Wen, M. T., Nowak, A., Wehner, B., Wiedensohler, A., Takegawa, N., Kondo, Y., Wang, X. S., Li, Y. P., Zeng, L. M., and Zhang, Y. H.: Variation of particle number size distributions and chemical compositions at the urban and downwind regional sites in the Pearl River Delta during summertime pollution episodes, Atmos. Chem. Phys., 10, 9431–9439, doi:10.5194/acp-10-9431-2010, 2010.

Yue, M. Z., Wang, Y. Z., Bian, S. F., Tian, S. L., and Lu, C.: Corrosion in the process of mixedly burning biomass with coal and preventive measures thereof, Thermal Power Generation, 40, 35–38, 2011.

Zhang, Y. H., Hu, M., Zhong, L. J., Wiedensohler, A., Liu, S.C., Andreas, M.O., Wang, W., and Fan, S. J.: Regional integrated experiments on air quality over Pearl River Delta 2004 (PRIDE-PRD2004): overview, Atmos. Environ., 42, 6157–6173, 2008a.

Zhang, Y. H., Su, H., Zhong, L. J., Cheng, Y. F., Zeng, L. M., Wang, X. S., Xiang, Y. R., Wang, J. L., Gao, D. F., Shao, M., Fan, S. J., and Liu, S. C.: Regional ozone pollution and observation-based approach for analyzing ozone-precursor relationship during the PRIDE-PRD 2004 campaign, Atmos. Environ., 42, 6203–6218, 2008b.

ACPD

12, 15639–15674, 2012

Table 1. Measured aerosol properties and meteorological parameters.

Property	Instrument	Relative humidity	Time resolution	Available data in days			
				Apr -09	Jul -09	Oct -09	Jan -10
1 $PM_{2.5}$ mass concentration	BGI Corporation, Model PQ200	40 %	23.5 h	30	31	31	31
2 OC/EC mass concentration	Atmoslytic Inc., Calabasas, CA, DIR model 2001 carbon analyzer	40 %	23.5 h	30	31	31	31
3 Water-soluble ions mass concentration	Dionex Corp, Sunnyvale, CA, Model Dionex 600	40 %	23.5 h	30	31	31	31
4 Total light scattering coefficient (450 nm, 550 nm, 700 nm)	TSI Performance Measurement Tools, Model 3563	17–73 %*	1 min	29	31	31	31
5 Particles number concentration in the range of 0.5–20 µm	TSI Aerodynamic Sizer, Model 3321	< 20%	5 min	30	30	29	30
6 Relative humidity	VASALA Model QMH102	29–88 %	30 min	30	31	31	31

* stands for the RH detected by a built-in RH sensor in Nephelometer.

ACPD
12, 15639–15674, 2012

Table 2. Optical parameters of chemical components for calculating the EORI.

component	ρ	n	k	component	ρ	n	k
$(NH_4)_2SO_4$	1.760	1.530	0.000	NH_4Cl	1.527	1.639	0.000
Na_2SO_4	2.680	1.480	0.000	NaCl	2.160	1.544	0.000
K_2SO_4	2.660	1.490	0.000	KCl	1.980	1.490	0.000
$MgSO_4$	2.660	1.560	0.000	$MgCl_2$	2.325	1.540	0.000
$CaSO_4$	2.610	1.570	0.000	$CaCl_2$	2.150	1.520	0.000
NH_4NO_3	1.725	1.554	0.000	POM	1.500	1.550	0.005
$NaNO_3$	2.261	1.587	0.000	EC	1.500	1.950	0.660
KNO_3	2.110	1.504	0.000	Water	1.000	1.333	0.000
$Mg(NO_3)_2$	2.020	1.510	0.000	Residual	2.300	1.620	0.000
$Ca(NO_3)_2$	2.504	1.530	0.000				

ACPD
12, 15639–15674, 2012

Table 3. Monthly average of the parameters required in the Mie Model.

Item	Apr-09	Jul-09	Oct-09	Jan-10
Ambient RH (%)	68.0 (11.9)	68.4 (8.2)	50.2 (12.4)	71.3 (14.3)
n_{eff}	1.483 (0.035)	1.495 (0.028)	1.538 (0.029)	1.490 (0.037)
k_{eff}	0.042 (0.011)	0.049 (0.013)	0.054 (0.012)	0.040 (0.010)
f_{eff}	1.222 (0.097)	1.196 (0.075)	1.093 (0.054)	1.212 (0.092)
$\rho_{\text{dry}}(\text{g cm}^{-3})$	1.799 (0.052)	1.861 (0.056)	1.833 (0.034)	1.851 (0.037)
$\rho_{\text{wet}}(\text{g cm}^{-3})$	1.455 (0.118)	1.515 (0.096)	1.646 (0.089)	1.493 (0.118)

Note: the data in brackets are referenced to the standard deviation.

ACPD
12, 15639–15674, 2012

Table 4. Parameter "a" and the R^2 of the curve fittings by Eq. (10).

Item	a	R^2	RH = 70 %	RH = 80 %	RH = 90 %
$h_{bep,pm0.5–2.5}$	−0.2964	0.9920	1.233 (0.050)	1.378 (0.075)	1.746 (0.147)
$h_{bsp,pm0.5–2.5}$	−0.3778	0.9953	1.315 (0.069)	1.514 (0.098)	2.020 (0.184)
$h_{bap,pm0.5–2.5}$	–	–	0.995 (0.029)	0.986 (0.040)	0.951 (0.066)
$h_{\omega\,0,pm0.5–2.5}$	−0.0811	0.9948	1.066 (0.017)	1.098 (0.022)	1.157 (0.032)

Note: the data in brackets are referenced to the standard deviation.

ACPD
12, 15639–15674, 2012

Table 5. Monthly average of $h_{bep,pm0.5–2.5}$, $h_{bsp,pm0.5–2.5}$, $h_{bap,pm0.5–2.5}$ and $h_{\omega 0,pm0.5–2.5}$.

Item	Apr-09	Jul-09	Oct-09	Jan-10
Ambient RH (%)	68.0 (11.9)	68.4 (8.2)	50.2 (12.4)	71.3 (14.3)
$h_{bep,pm0.5–2.5}$	1.265 (0.192)	1.236 (0.128)	1.041 (0.091)	1.275 (0.171)
$h_{bsp,pm0.5–2.5}$	1.354 (0.258)	1.343 (0.188)	1.056 (0.118)	1.369 (0.229)
$h_{bap,pm0.5–2.5}$	1.004 (0.029)	0.985 (0.035)	0.995 (0.010)	0.993 (0.020)
$h_{\omega 0,pm0.5–2.5}$	1.064 (0.040)	1.083 (0.041)	1.012 (0.026)	1.069 (0.040)

Note: the data in brackets are referenced to the standard deviation.

ACPD
12, 15639–15674, 2012

Table 6. Results of the Mie Model estimation and the relevant calculations.

Item	Apr-09	Jul-09	Oct-09	Jan-10
Ambient RH (%)	68.0 (11.9)	68.4 (8.2)	50.2 (12.4)	71.3 (14.3)
m_{total} ($\mu g\,m^{-3}$)	125.3 (48.5)	61.6 (17.5)	108.9 (48.7)	149.8 (80.4)
$b_{\text{sp,total}}$ (Mm^{-1})	360.3 (150.5)	123.1 (48.5)	494.9 (254.5)	633.7 (354.4)
$b_{\text{ap,total}}$ (Mm^{-1})	62.4 (21.7)	35.4 (11.7)	63.0 (25.2)	73.3 (42.1)
$b_{\text{ep,total}}$ (Mm^{-1})	422.7 (168.3)	158.5 (58.4)	557.9 (275.0)	707.0 (393.6)
ω_0	0.84 (0.04)	0.77 (0.04)	0.88 (0.02)	0.89 (0.02)
$\mathring{a}_{450/700}$	1.47 (0.18)	1.77 (0.13)	1.79 (0.13)	1.79 (0.20)
$e_{\text{sp,total}}$ ($m^2\,g^{-1}$)	11.1 (1.4)	9.1 (0.7)	12.2 (1.1)	12.4 (0.8)
$e_{\text{ap,total}}$ ($m^2\,g^{-1}$)	2.4 (0.4)	2.7 (0.4)	2.7 (0.4)	2.4 (0.3)

Note: the data in brackets are referenced to the standard deviation.

ACPD
12, 15639–15674, 2012

Fig. 1. Satellite photo of the monitoring site and surroundings (from Google Earth).

ACPD
12, 15639–15674, 2012

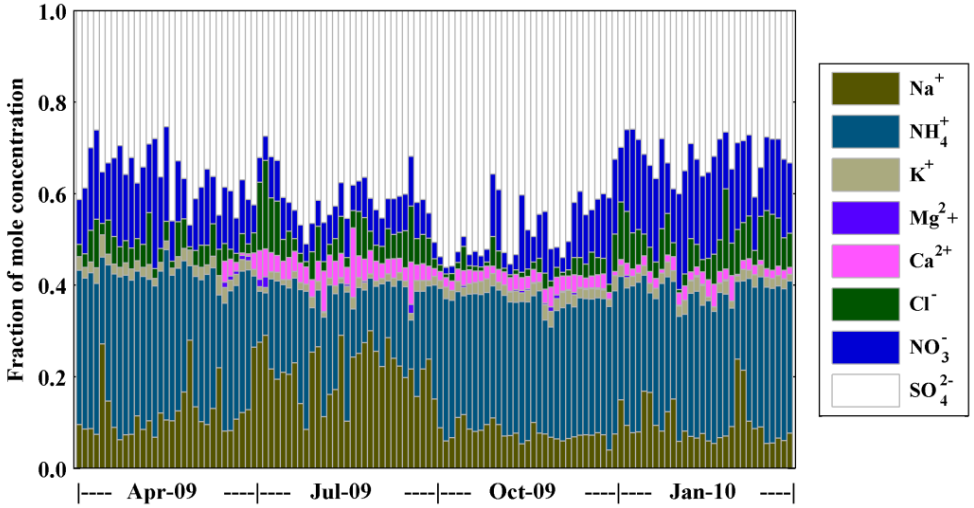

Fig. 2. Temporal variation of the identified water-soluble ions in mole proportion.

ACPD
12, 15639–15674, 2012

Impact of relative humidity and particles size distribution

Z. J. Lin et al.

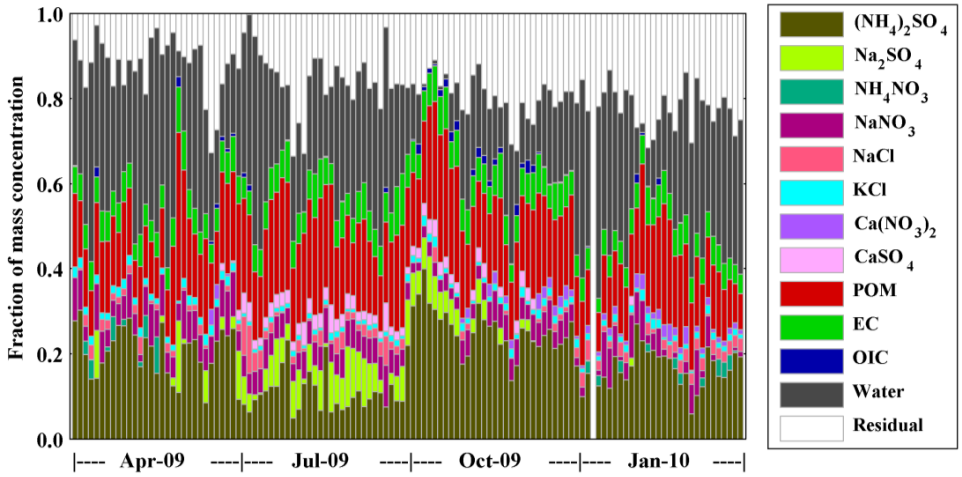

Fig. 3. Temporal variation of the chemical components in mass proportion. Note: OIC mean the other determined inorganic salts.

ACPD
12, 15639–15674, 2012

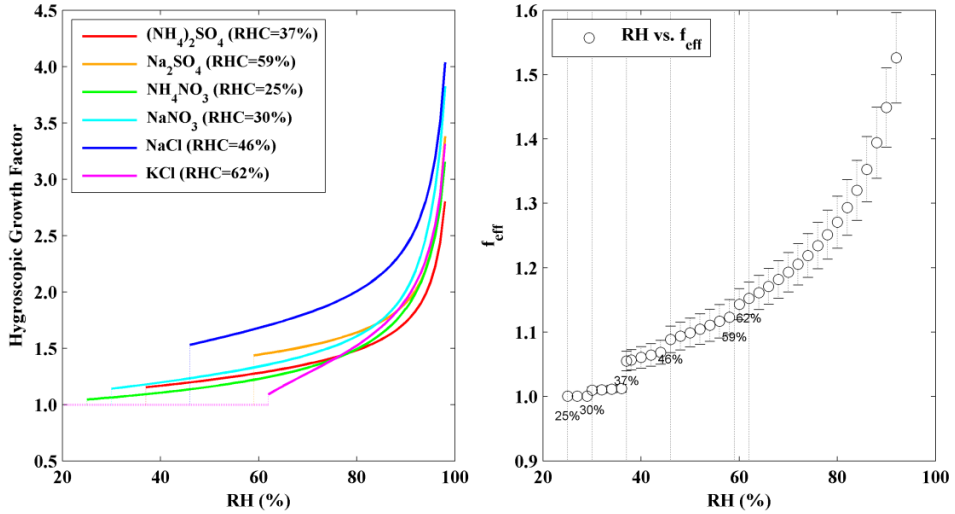

Fig. 4. RH dependence curve of some inorganic salts and the EGF. Note: the bars in the right figure stand for the standard deviation of f_{eff} at specified RH.

ACPD
12, 15639–15674, 2012

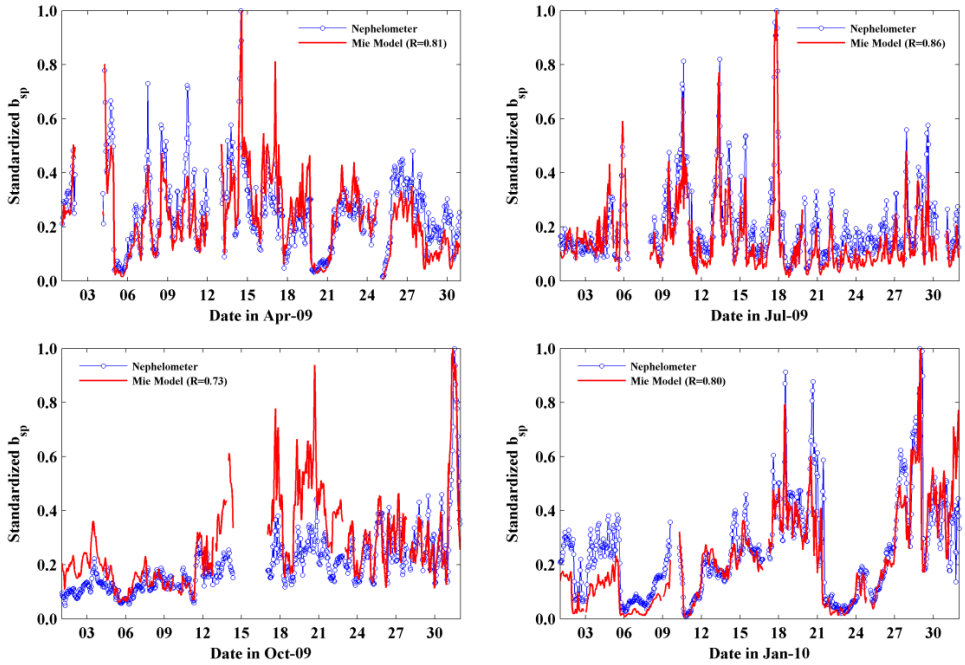

Fig. 5. Temporal variations of the $b_{sp,pm0.5–2.5}$ and $b_{sp,neph}$. Note: standardized b_{sp} is the ratio of individual b_{sp} to their maximum.

ACPD
12, 15639–15674, 2012

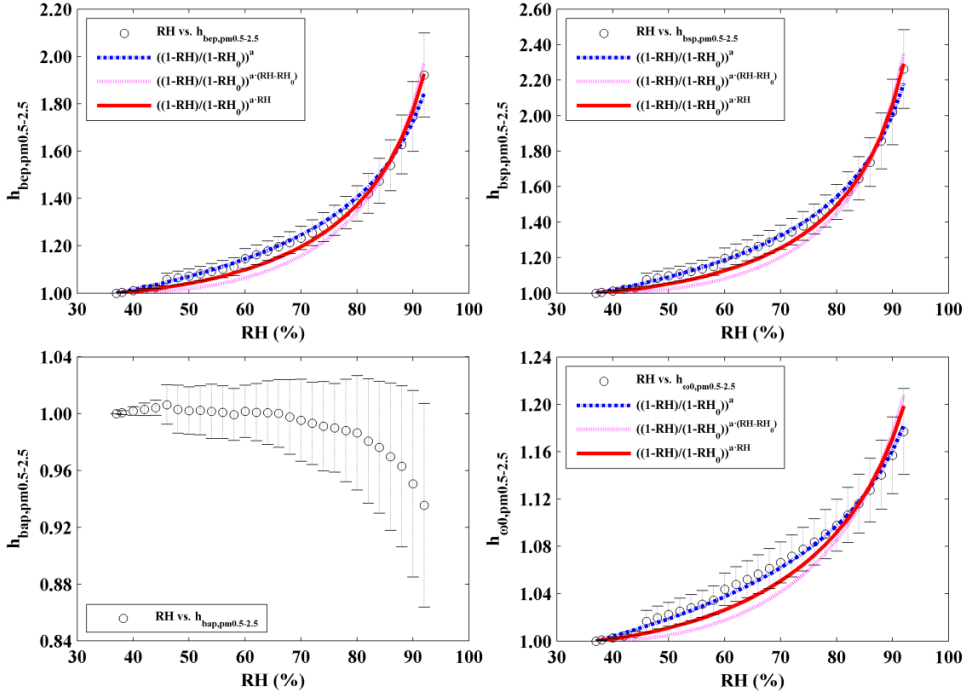

Fig. 6. RH dependence curve of $h_{\mathrm{bep,pm0.5–2.5}}$, $h_{\mathrm{bsp,pm0.5–2.5}}$, $h_{\mathrm{bap,pm0.5–2.5}}$ and $h_{\omega\mathrm{0,pm0.5–2.5}}$. Note: the bars in the figure stand for the standard deviation of h_{Y} at specified RH.

ACPD
12, 15639–15674, 2012

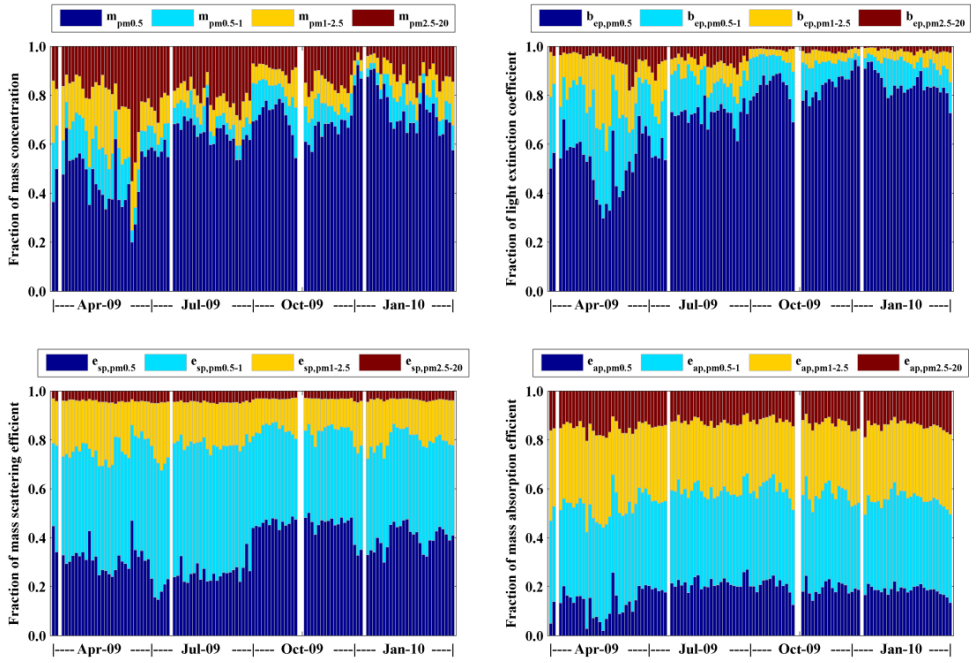

Fig. 7. Temporal variation of size distribution of mass concentration and optical properties.

ACPD
12, 15639–15674, 2012